



**HAL**  
open science

## Anthropogenic modification of a giant ground sloth tooth from Brazil supported by a multi-disciplinary approach

Thaís R Pansani, Loïc Bertrand, Briana Pobiner, Anna K Behrensmeyer, Lidiane Asevedo, Mathieu Thoury, Hermínio I Araújo-Júnior, Sebastian Schöder, Andrew King, Mírian L. A. F. Pacheco, et al.

► **To cite this version:**

Thaís R Pansani, Loïc Bertrand, Briana Pobiner, Anna K Behrensmeyer, Lidiane Asevedo, et al.. Anthropogenic modification of a giant ground sloth tooth from Brazil supported by a multi-disciplinary approach. *Scientific Reports*, 2024, 14 (1), pp.19770. 10.1038/s41598-024-69145-5 . hal-04685706

**HAL Id: hal-04685706**

**<https://hal.science/hal-04685706v1>**

Submitted on 3 Sep 2024

**HAL** is a multi-disciplinary open access archive for the deposit and dissemination of scientific research documents, whether they are published or not. The documents may come from teaching and research institutions in France or abroad, or from public or private research centers.

L'archive ouverte pluridisciplinaire **HAL**, est destinée au dépôt et à la diffusion de documents scientifiques de niveau recherche, publiés ou non, émanant des établissements d'enseignement et de recherche français ou étrangers, des laboratoires publics ou privés.




Distributed under a Creative Commons Attribution - NonCommercial - NoDerivatives 4.0 International License



OPEN

# Anthropogenic modification of a giant ground sloth tooth from Brazil supported by a multi-disciplinary approach


Thaís R. Pansani<sup>1,2,3</sup>, Loïc Bertrand<sup>3</sup>, Briana Pobiner<sup>1</sup>, Anna K. Behrensmeyer<sup>4</sup>, Lidiane Asevedo<sup>5</sup>, Mathieu Thoury<sup>6</sup>, Hermínio I. Araújo-Júnior<sup>7</sup>, Sebastian Schöder<sup>8</sup>, Andrew King<sup>8</sup>, Mírian L. A. F. Pacheco<sup>9</sup> & Mário A. T. Dantas<sup>5</sup>

Identifying evidence of human modification of extinct animal remains, such as Pleistocene megafauna, is challenging due to the similarity of anthropogenic and non-anthropogenic taphonomic features observed under optical microscopy. Here, we re-investigate a Late Pleistocene ground sloth tooth from northeast Brazil, previously suggested as human-modified based only on optical observation. To characterize the macro- and micro-morphological characteristics of the marks preserved in this tooth and evaluate potential human modification, we used stereomicroscope and scanning electron microscopy (SEM) supplemented by energy dispersive spectroscopy (EDS), UV photoluminescence (UV/PL), synchrotron-based X-ray fluorescence (SR-XRF), and synchrotron micro-computed tomography (SR- $\mu$ CT). These methods allowed us to discriminate non-anthropogenic taphonomic features (root and sedimentary damage), anthropogenic marks, and histological features. The latter shows the infiltration of exogenous elements into the dentine from the sediments. Our evidence demonstrates the sequence of anthropogenic and non-anthropogenic taphonomic modification of this tooth and supports its initial intentional modification by humans. We highlight the benefits of emerging imaging and spectral imaging techniques to investigate and diagnose human modification in fossil and archaeological records and propose that human modification of tooth tissues should be further considered when studying possibly anthropogenically altered fossil remains.

**Keywords** Pleistocene, South America, Zooarchaeology, Megafauna, Tooth artifact

The reconstruction of ancient human relationships with extinct animals relies on the nature and timing of certain activities that can be identified as zooarchaeological. Some examples are butchery and other marks linked to human subsistence or additional cultural activities on animal remains, including scraping marks, hole perforations, burning damage, or use-wear traces preserved in ancient bones, shells, and teeth<sup>1–5</sup>.

Identifying traces of human modification preserved in fossilized bones and distinguishing them from non-human modification traces is not an easy task. Trampling marks can mimic cut marks<sup>6</sup>, sedimentary abrasion can obscure or destroy diagnostic features of anthropogenic marks<sup>1,6</sup>, and diverse biotic agents (e.g., carnivores, rodents, microorganisms, plant roots) can damage fresh and fossil bones and teeth in ways that mimic or overprint anthropogenic traces<sup>5,7,8</sup>. Additionally, different tools and technologies used during ancient human processing activities, as well as the mechanical properties of stone tool edges and the hardness of the bone surface itself, can affect the morphological features of distinct anthropogenic marks<sup>9</sup>.

<sup>1</sup>Department of Anthropology, National Museum of Natural History, Smithsonian Institution, Washington, DC, USA. <sup>2</sup>Programa de Pós-Graduação em Ecologia e Recursos Naturais, Universidade Federal de São Carlos, São Carlos, SP, Brazil. <sup>3</sup>Université Paris-Saclay, ENS Paris-Saclay, CNRS, PPSM, Gif-sur-Yvette, France. <sup>4</sup>Department of Paleobiology, National Museum of Natural History, Smithsonian Institution, Washington, DC, USA. <sup>5</sup>Laboratório de Ecologia e Geociências, Instituto Multidisciplinar em Saúde, Universidade Federal da Bahia, Vitória da Conquista, BA, Brazil. <sup>6</sup>Institut photonique d'analyse non-destructive européen des matériaux anciens, Université Paris-Saclay, CNRS, ministère de la Culture, UVSQ, MNHN, Saint-Aubin, France. <sup>7</sup>Departamento de Estratigrafia e Paleontologia, Faculdade de Geologia, Universidade do Estado do Rio de Janeiro, Rio de Janeiro, RJ, Brazil. <sup>8</sup>Synchrotron Soleil, Gif-sur-Yvette, France. <sup>9</sup>Laboratório de Paleobiologia e Astrobiologia, Departamento de Biologia, Universidade Federal de São Carlos, Sorocaba, SP, Brasil. email: rabitopansanit@si.edu

The study of surface modifications on animal remains using traditional methods, such as stereomicroscopic and scanning electron microscopy (SEM) imaging, has been useful over the past decades<sup>2,10,11</sup>, but it can also be problematic due to subjective interpretations by different taphonomists<sup>3,6,12,13</sup>. Additional scientific approaches, especially using more high-resolution three-dimensional data capture and analysis techniques (e.g.,<sup>14,15</sup>) have reduced subjectivity in interpreting causes of bone modification.

Many Brazilian megafauna fossils come from fossiliferous deposits referred to as natural tanks in northeast Brazil (Fig. 1). These are natural depressions where seasonal rainwater can accumulate, producing Quaternary sedimentary deposits that commonly preserve Late Pleistocene megafauna<sup>16</sup>. In the original biocoenosis, natural tanks were valuable water sources for megamammals and, when dried out, they were sites where skeletal remains could accumulate and be buried by debris-flow or other sedimentary events<sup>17</sup>.

Dantas et al.<sup>18,19</sup> previously suggested human modification of a fragmentary molariform tooth of the giant ground sloth *Eremotherium laurillardii* (Lund, 1842) from a tank on a farm in Poço Redondo, Sergipe state, northeast of Brazil (Fig. 1A, B). The tooth was radiocarbon dated to the Late Pleistocene (updated here to 13,810–13,950 calibrated years before the present (cal yr B.P.) based on the methodology proposed by Dantas and Cherkisky<sup>20</sup> to convert radiocarbon ages performed on bioapatite). The tooth was found with other megamammal fossils, including megatheriids, mylodontids, scelidotheriids, glyptodonts, pampatheriids, toxodonts, gomphotheriids, equids, macraucheniiids, camelids, and felids<sup>21</sup>, as well as with lithic artifacts<sup>18</sup>. Lithics could not be collected due to legal restrictions at the site, and only taxonomic<sup>21</sup> and paleoecological<sup>22,23</sup> studies have been performed in this area. Primary stratigraphic information on these fossils is lacking, as they were removed from their original context and deposited in the area adjacent to the tank by unrecorded earlier (human) activities. Hence, there are no ages available based on archaeological context, which makes it hard to identify the timing of any human alteration carried out on a fossil, despite the age obtained for this tooth.

Anthropogenic modification was originally interpreted based on the unusual triangular shape of this tooth in comparison with the natural cylindrical shape of ground sloth molariform teeth (Fig. 1C); one side presenting a

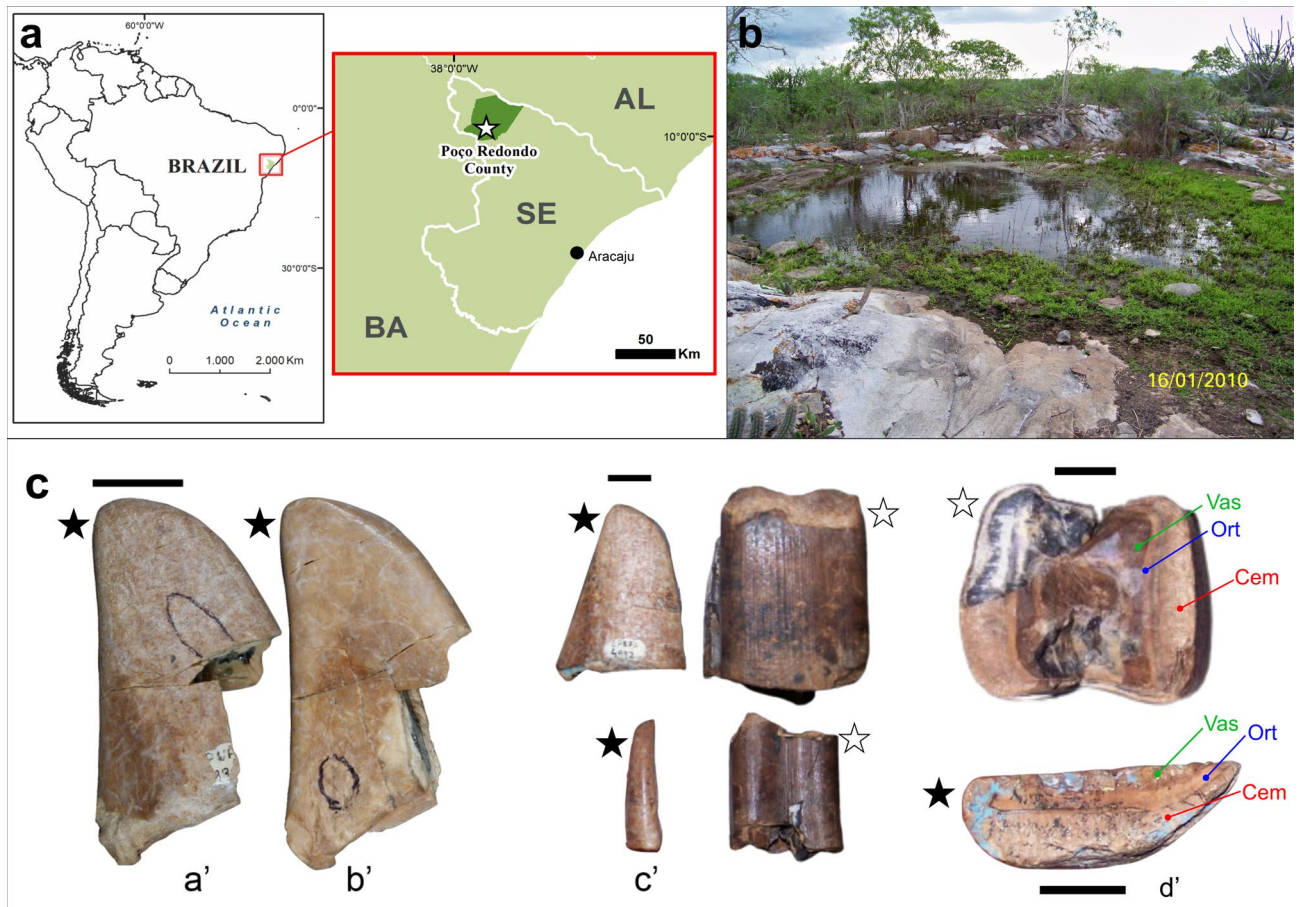


**Figure 1.** Study area and fossil material. (a) Map of the location of the tank deposit where the tooth was found, in Poço Redondo, Sergipe state, northeast Brazil. (b) Photograph of the tank environment during the rainy season. (c) Macroscopic images of the external (a'), internal (b'), lateral (c'), and transversal (d') views of the modified ground sloth tooth analyzed in this study (LPUFS 4992; referenced by black stars). Notice the remarkable difference between the modified tooth and another *E. laurillardii* molariform fragment (M4, LPUFS 1873; referenced by white stars) in (c') and (d'). Notice distinguishable cement (Cem), vasodentine (Vas), and orthodentine (Ort) layers, characteristic of Megatheriidae teeth in (d'); modified from Dantas et al.<sup>18</sup>. Scale bars: 1 cm.

smoother surface than the other; and the presence of parallel marks on the smooth side. Previous images (digital microscopy, 200× and 500× magnification) combined with the lack of taphonomic contextual information from preliminary studies generated doubt about this diagnosis and the supposed human modification of this tooth<sup>24</sup>.

We acknowledge that identifying human activity in fossil remains without context or from disturbed sites is problematic, especially when debating the contentious topic of megafauna exploitation in the Americas. However, we regard careful evaluation of potential causal agent(s) of these fossil modifications as important in providing examples of methodological solutions for robust taphonomical characterizations in paleontology and zooarchaeology. Here we test a more in-depth analysis of this specimen, including 2D and 3D microscopic and elementary characterization of the tooth surface. This multi-technique approach provided more data on these marks that clarifies the possibility of human intentional actions on this fossil from Poço Redondo.

## Results

We analyzed the molariform tooth according to a carefully designed protocol in order to extract as much information as possible from the fossil. Considering the quality and robustness of the data, the protocol proposed here also took into account the limitations and complementarities between the analytical techniques (Fig. 2). First, we characterized the sample by naked eye, observing the general shape, color, and preserved marks. The tooth is remarkably distinct from the original anatomical condition of *E. laurillardi* molariforms, which can be, in occlusal view, triangular (first upper molariform tooth), trapezoidal (second to fourth upper molariform teeth, and all lower molariform teeth) or square (fifth upper molariform tooth)<sup>25,26</sup>; (Fig. 1C).

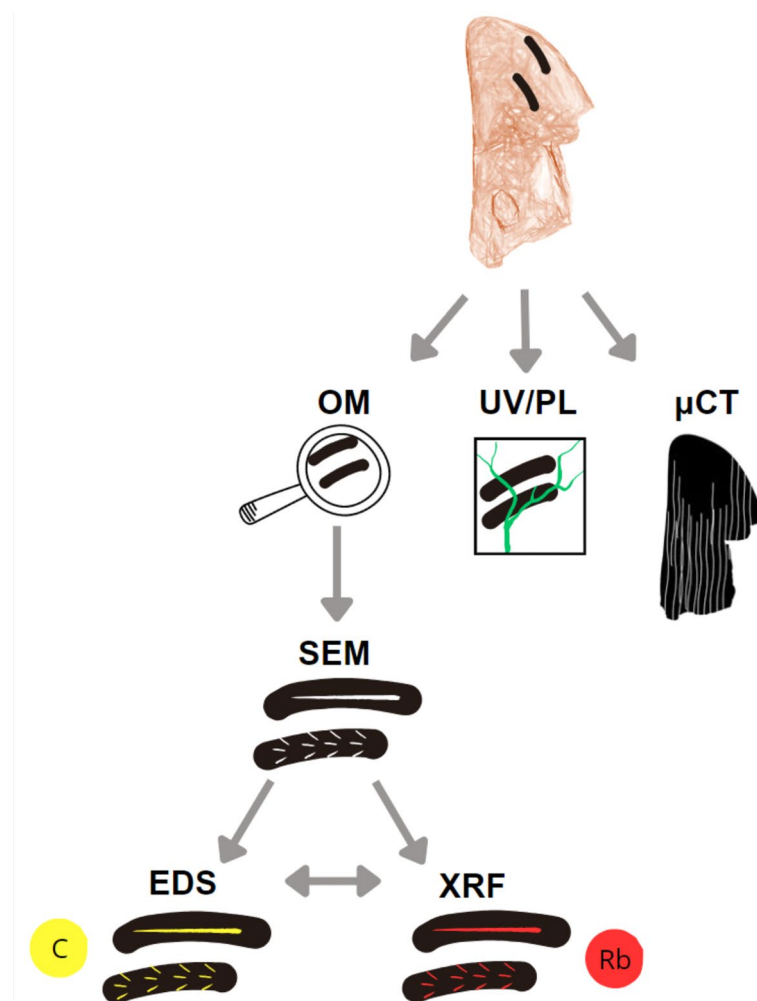


**Figure 2.** Graphical abstract summarizing the protocol we explored in this study. Optical microscopy serves as a general characterization of areas of interest and  $\mu$ CT allows three-dimensional reconstruction of the sample and acquisition of histological information. Taphonomic signatures can be analyzed in higher magnifications using SEM, and chemically characterized using EDS and XRF. EDS and XRF are complementary to each other: while EDS allows the identification of lighter elements (e.g., C), XRF allows the identification of heavier and trace elements (e.g., Rb). UV/PL complements both imagining and chemical characterization, providing information on the morphology and orientation of taphonomic signatures as well as revealing the overlap of features (e.g. mineralized tissue and organic matter).

Optical microscopy helped in the general characterization of areas of interest, which were then analyzed in higher magnifications using SEM and  $\mu$ CT (synchrotron-based microtomography). We did not observe features of recent marks on this tooth that usually result from excavation or laboratory preparation, such as distinct colors in the modification marks compared with the adjacent surface, and microscopic criteria including transverse micro-flakes and internal flakes within such marks<sup>27</sup>. Evidence of rodent gnawing, carnivore gnawing, digestion dissolution, and insect damage were also not observed.

Macroscopic observation showed distinct surface marks similar to root marks on the tooth surface (Fig. 1C). The BSE-SEM imaging confirmed that these marks show a darker color than the dentine's surface, indicating lighter elemental composition, possibly organics (Fig. 4I). The EDS analysis confirms the high concentration intensities of C as well as Ca and P in the area analyzed (Fig. S1; supplementary material).

The non-anthropogenic modifications also were characterized morphologically by  $\mu$ CT (Fig. 3) and morphologically and compositionally by PL (Fig. 4). We identified the main intersecting micro-taphonomic signatures and histology. We reconstituted three-dimensional aspects of the tooth shape at the same time we accessed micro marks (Fig. 3). We also verified a parallel arrangement of mark structures on the tooth's lateral edges (in the cementum layer), previously misidentified as anthropogenic marks, and now described as dentinal tubules, corroborated by  $\mu$ CT analysis.

We identified sets of parallel marks with similar sizes and widths using SEM (Fig. 5I). The characterization of these marks gained in-depth resolution through  $\mu$ CT and PL (Figs. 3D, 4A–B). PL highlighted their standard orientation following the curvature of the movement in the rounded edges of the tooth (Fig. 4A–B). Besides the homogenous and matte coloration of the identified anthropogenic marks and the tooth surface, PL and SEM–EDS showed that some anthropogenic marks are overlapped by other non-anthropogenic taphonomic signatures (e.g.,

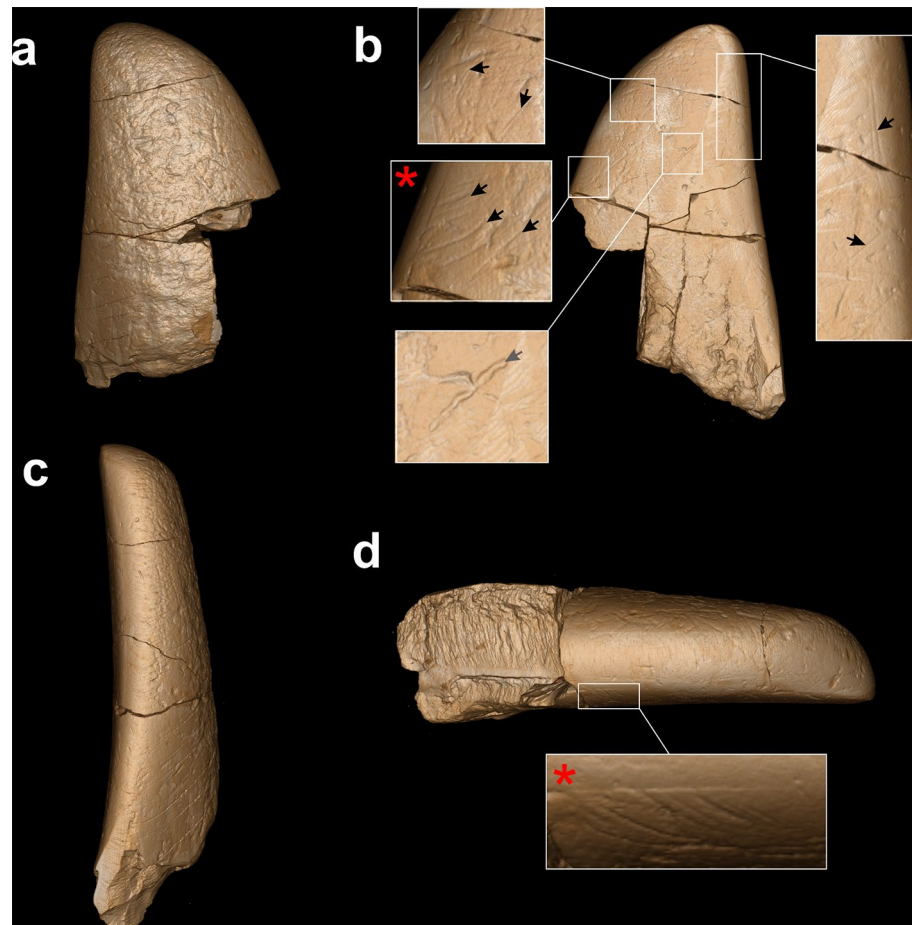


**Figure 3.** 3D reconstruction of the modified molariform tooth from synchrotron micro-computed tomography. Notice the three-dimensional morphology of diverse surface modifications along the specimen. (a) External view. (b) Internal view with zoomed in areas where black arrows indicate anthropogenic multi-oriented striations and green arrow indicates root damage. Notice the distinct rough aspect of the tooth surface in the external view and the smooth aspect in the internal view. (c, d) Lateral view where the histological features are exposed. Red asterisks in (b) and (d) indicate the same anthropogenic signatures observed from different angles. (See also Fig. 1).

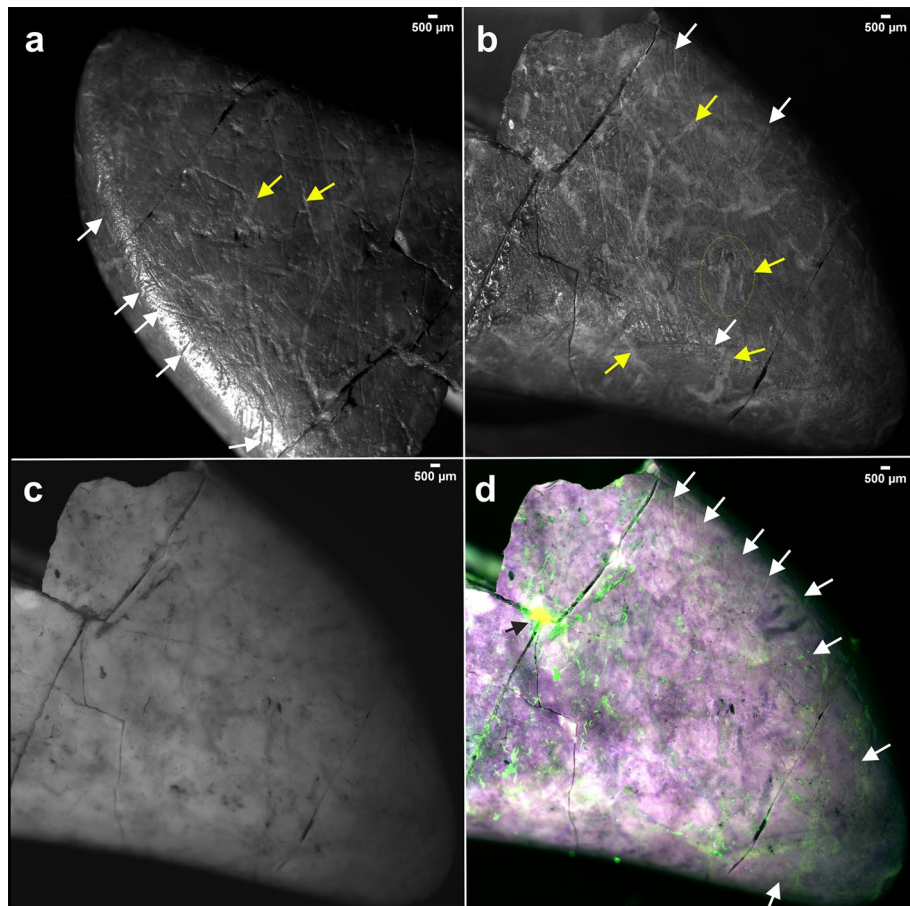


**Figure 4.** Photoluminescence images of the internal view of the tooth under distinct excitation and emission wavelengths. (a) and (b) An abundance of multi-oriented scratches along the center of the surface and the curvature area of the tooth, some overlapped by root marks. The short, clustered, and parallel marks following specific orientations and the presence of straight linear marks and perpendicular and crossed striations characterize anthropogenic intervention. The edge of the tooth shows some specular reflections because the surface is smooth, and this area acts as a mirror. (c) Post-depositional damage, predominantly composed of root marks. (d) False-color reconstructed image enables visualization of the location and orientation of anthropogenic and non-anthropogenic taphonomic marks. For all images: white arrows indicate sets of deep and wide anthropic marks (possibly grinding traces?) around concave areas; yellow marks indicate root marks, and the yellow circle indicates the pitting damage associated with root marks (probably acid corrosion from the roots); the area luminescing in the  $472 \pm 15$  nm spectral range (black arrow in (d)) coincides with a consolidated area and is attributed to remains of recent organic glue.

root and chemical damage, trampling marks, and sedimentary abrasion; Figs. 4B, D, 5B, D, I). The anthropogenic marks and surrounding area of the tooth show uniform color aspects, revealing uniform density among them. The bioapatite surface with brighter/grey color characterizes heavier density, and the overlaid, darker damage features characterize lighter density (i.e., organic matter). EDS analysis in this area shows a predominance of the elements Ca, C, O, and P (Fig. S1; supplementary material).

SEM micrographs of the internal view of the tooth (vasodentine; Fig. 1C-b') show a damaged area that exposes the internal dentine microstructure (Fig. 6F–J; Fig. S2, supplementary material), identified as natural casts of dentinal tubules in the orthodentine. EDS analysis confirms the chemically altered state of this region by Al and Si infiltrations (Fig. 6H–I). Organic matter, characterized by carbon content, overlaps such ancient damage (Fig. 6G). Dentinal tubules from the lateral view (Fig. 6C-c') also show infiltration of Al and Si. SEM–EDS analyses were complemented by the higher efficiency of X-ray fluorescence (XRF), and revealed residues of sediments (Fig. 6G–J) and chemical infiltrations by weathering and diagenesis elements (Al, Si, Fe, Rb, and Sr) on these histological structures (Figs. 6A–E and 7).

## Discussion

The study of causes of post-mortem modification features of teeth and bones is a challenge for taphonomy, since many environmental processes can mimic marks of human action. The archaeological context does not always constitute favorable evidence for determining the age at which an object was transformed into an artifact. This

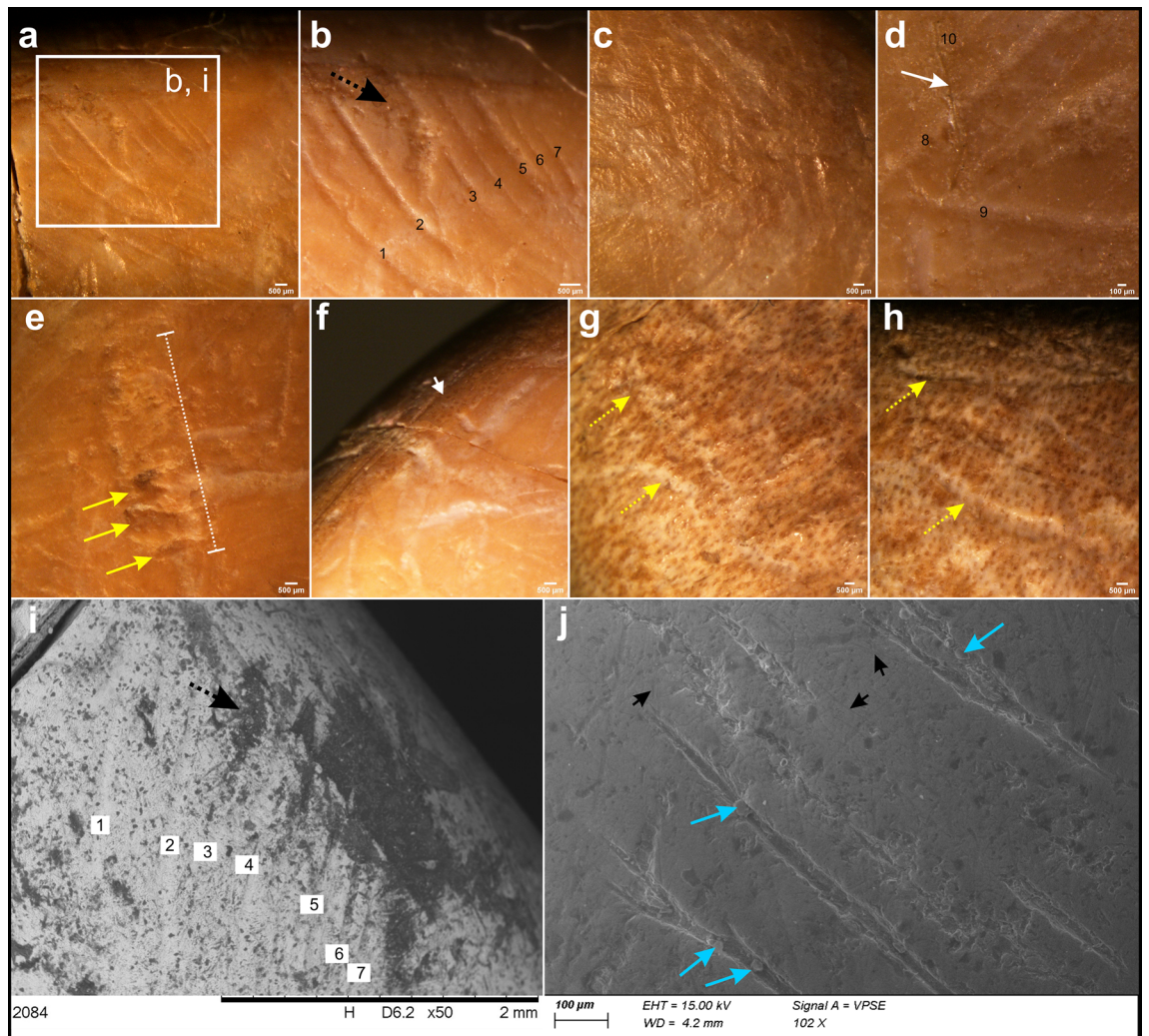


**Figure 5.** Stereomicroscopic images of the tooth. (a–f): Internal view. (a) Set of short parallel linear marks of similar width and length, following the curvature of the tooth. The white square containing 7 linear marks is zoomed in (b), where root damage (black dotted arrow) overlaps the ancient marks. (c) Superficial and multi-oriented striations provide a polished aspect to this side of the tooth. (d) An elongated mark with irregular (sinuous) trajectory (mark 10, indicated by the white arrow), characteristic of sedimentary abrasion or trampling marks, overlapping an ancient and notably wider mark (mark 9). (e) Root etching, with total damage indicated by the dotted white line, and three pitting fissures indicated by yellow arrows, which we interpret as corrosion caused by root acids. (f) Clear distinction of both sides of the tooth, with the internal view smoother than the external view. Shallow elongated marks, as indicated by short white arrow, can be result of trampling or sedimentary abrasion. (g) and (h) External view. Moderate root damage is indicated by the yellow dotted arrows. (i) BSE-SEM image of the squared area in (a). Notice the recent root damage (black dotted arrow) in (b) optically black, indicating high organic content, overlapping the marks with uniform contrast between their interior and the adjacent surface, indicating simultaneous mineralization. (j) Close up of the dentinal tubules acquired in the lateral view of the tooth. Image acquired with SEM using VPSE detector. Notice residues of sediments inside the histological structures (blue arrows), indicating their exposure before/during burial. Sedimentary abrasion marks along the tooth surface are very fine, shallow, and sinuous (see examples indicated by short black arrows).

is the case of the tank at the Poço Redondo farm, where the giant sloth tooth was found. Even given the dating of the sample, the possibility of temporal mixing in the tank calls into question the age of modification of this tooth as an artifact. However, because this fossil tooth is a specimen with intriguing archaeological implications, especially for the study of human-megafauna interaction in Pleistocene South America, we investigated possible anthropogenic nature of its modifications.

The surface of the tooth (internal view) has multiple modifications interpreted as possible to desiccation cracks, root marks, acid damage, and sediment abrasion marks (Fig. 1Cb'). In addition to these, we observed regular and parallel deep marks in concave areas of the tooth, and transversal and multi-oriented striations compatible to anthropogenic marks (Fig. 4).

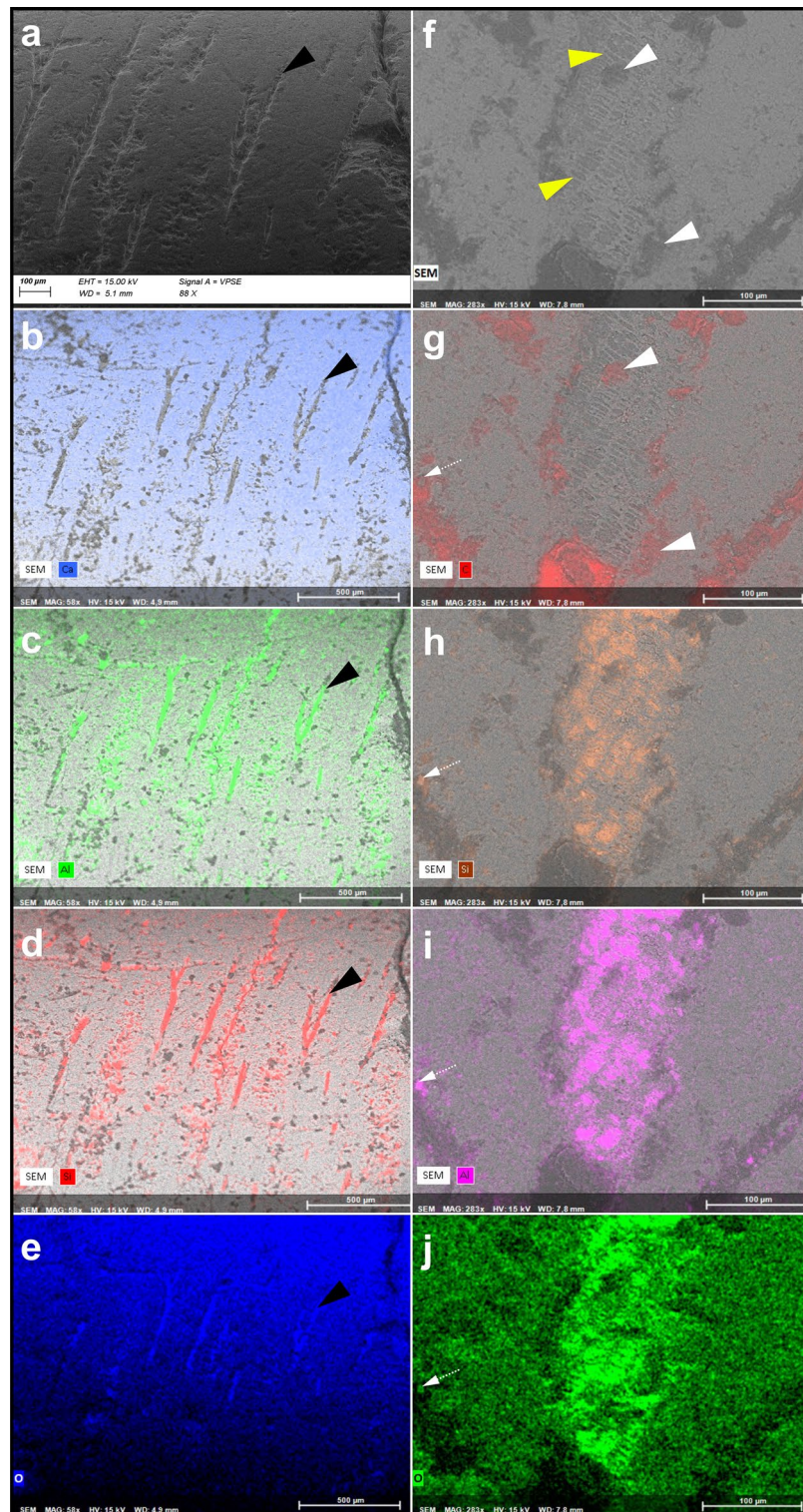


**Figure 6.** SEM and EDS images of two different areas of the tooth. (a–e) SEM and artificially colored EDS images from the lateral view of the tooth. (a) Image collected with VPSE detector. Notice the exposure of histological structures (dental tubules), also distinguished through microCT (Fig. 3C). (b–e) Distinct patterns among the elements Ca, Al, Si, and O, respectively. False colors highlight the depletion of Ca and the incorporation of Al, Si, and O in these structures. Black arrows in each photo indicate the same structure for reference. (f–i) SEM–EDS images of a damaged area on the internal view of the tooth. (f) Notice exposed dental tubules from the orthodontine layer, indicated by yellow arrows, as well as specific darker zones in BSE–SEM (indicated by white arrows), demonstrating higher organic composition due to contrasting electron density with the bone bioapatite. This is corroborated by the EDS detection of its carbon composition in (g). (h–j) Distinct diagenetic patterns based on the local distribution of Si, Al, and O, respectively. We can observe that Si, Al, and O are associated with the damage that exposes the histological structures, which also overlaps the carbon-rich taphonomic features (see grains indicated by the dotted white arrow).



Physical abrasion (e.g., from water transport with sediment) was first considered as a cause of the change in shape and rounded edge of the tooth. While abrasion rounding is more commonly recognized in bones, teeth (with and without enamel) can also become rounded through these processes<sup>5,28</sup>. We assume that the distinct “triangular” shape of the tooth fragment, with one clearly rounded edge (Fig. 1C) is unlikely to have resulted from fluvial transport mainly because 1) its pointed shape with two distinct surface textures, and 2) sedimentary abrasion produces randomly oriented, and fine shallow marks with non-straight trajectories<sup>12,29</sup>. These differ markedly from the sets of parallel scratches with similar orientation and short wide linear marks observed in the internal view of the tooth (Figs. 3B, 4A–B, 5I). This fine-scale analysis also gains support for anthropogenic marks based on comparative observations of the Smithsonian’s National Taphonomic Reference Collection (NTRC) (Table 1; Fig. S3; supplementary material). The range of methods we utilized (see “Methods”) tested for different types of anthropogenic and non-anthropogenic processes, noting also superimposed features that could indicate the sequence of different modifications in time (e.g., anthropogenic marks before root marks and sedimentary abrasion; Figs. 4 and 5).

Fig.	Technique/method	Information	Significance	Limitations	Surface modification and macro-taphonomic signatures	Micro-taphonomic signatures and mineralogy	Histological features
Figure 1C	Macro-observation	Overall shape compared with unaltered tooth, color observation of tooth surface, and macro-taphonomic signatures		Likely to misinterpret non-anthropogenic and anthropogenic modifications in lack of an in-depth study	X		
Figure 5A–H	Stereomicroscopy	General characterization of surface modifications (marks, color, some minerals)	Delimitation of interest areas for imaging studies in higher magnifications	Limited focus and magnification. Hard to observe overlaps among different sequences of taphonomic signatures	X		
Figure 3	Synchrotron $\mu$ CT	Internal micro-structure, histology, topography/texture of the tooth surface and marks	3D reconstruction of the sample, 3D observation of taphonomic signatures	Restrict access to synchrotron facilities worldwide	X	X	X
Figure 4	Photoluminescence (UV/PL)	Location, orientation, and overlapping of anthropogenic and other taphonomic signatures	Possible to observe the pattern distribution of different marks of interest separately and the overlapping of taphonomic signatures that can support the sequence of taphonomic events	Only qualitative data	X	X	
Figure 5I–J	Scanning electron microscopy (SEM)	Ultra characterization of surface modifications in higher magnifications (microscopic details, micromorphology, topography of marks, mineral inclusions)	Enables micro-morphological, micro-structural, and topographic observation	Electron charger can hinder image interpretation, difficult to capture surface details in irregular textures, electron charging	X	X	X
Figure 6	Energy dispersive spectroscopy (EDS)	Chemical characterization of tooth surface and taphonomic signatures	Detection of chemical elements and their intensities. Chemical identification helps to characterize abrasions, corruptions, and mineral precipitation, which can be useful to complement SEM and PL/UV imaging and reconstitute the taphonomic history of the sample	Detection of most light elements, with a limit for heavy trace elements and rare earth elements	X		
Figure 7	Synchrotron X-ray fluorescence (XRF)	Chemical characterization of tooth surface and taphonomic signatures	Identification of elements in mineralized tissues. Detection of heavy trace elements and rare earth elements that can help the interpretation of preservation aspects	Usually not efficient in the detection of lighter elements. Synchrotron micro-XRF are restricted to synchrotron facilities worldwide	X	X	

**Table 1.** Summary of information acquired on different taphonomic features using each technique/method in this study.

We ruled out rodent gnawing marks as a source of scratches on the tooth because (1) rodents tend to gnaw bones, rather than teeth<sup>30</sup>; and (2) rodent gnawing marks generally flatten the bone and are morphologically broad, parallel paired, flat-bottomed grooves<sup>31</sup>. Unlike rodent and carnivore gnawing, the marks on this tooth are not U-shaped. Unlike trampling marks, they are not randomly orientated nor do they present asymmetrical edges and other characteristic features for trampling on teeth, such as ‘fork-ends’ or ‘tick-ends’ on their striae<sup>32</sup>. The marks observed on this tooth do not refer to dietary signatures, which are usually interpreted through dental microwear analysis, as these marks are localized on the lateral side of the dentin and not on its occlusal surface (Fig. 1C). Therefore, we interpret the intensive polish and reshaping of the tooth as the result of human modification. Although we did not observe internal microstriations in the anthropogenic marks, their presence or absence, at least in bone surface modifications, does not necessarily exclude anthropogenic origin. Microstriations are uncommon, for example, in chopping marks<sup>10</sup> and can also be observed in trampling marks<sup>12</sup>. Also, diagnostic features of anthropogenic marks can be erased by other taphonomic processes, including sedimentary abrasion<sup>6</sup>. Human-made marks might show distinct micro-morphologies from tools associated with different activities or raw materials<sup>9</sup>, thus we should not expect to find internal features of marks made by butchery on bones to be exactly similar to those made by intentional abrasion and reshaping of teeth.

Root damage identification relies on the meandering, multi-directional, deeply etched, and dendritic patterning and morphology of these marks<sup>31</sup>, as well as the lack of star-shaped pits, which are indicative of insect damage<sup>33</sup>. Some irregular pits are observed on the tooth surface, with similar morphology and sizes to experimental sedimentary damage on teeth<sup>32</sup>. We interpret three deep fissures (Fig. 5E) as the result of corrosion from the mycorrhizal acidification commonly associated with growing roots, a process that secretes acids that can dissolve the bone and tooth matrix<sup>10</sup>.

The overlapping of organic (non-human) taphonomic signatures with the anthropogenic marks corroborates a sequence of the biostratigraphic events in which anthropogenic marks occurred before burial and posterior organic damage (Figs. 4 and 5). The detectable PL signals allowed observation of different types of pattern distributions on the tooth surface. False-color images highlight the different contrast between the mineralized dentine, ancient marks, overlapping ancient organic matter on the surface, and superficial recent organic contamination (Fig. 4D). Therefore, these plant signatures can be recent and may have occurred when the tooth and other fossils were excavated from the tank and deposited in the adjacent area before paleontological rescue, as subaerial recent plant growth can also damage fossilized remains<sup>5</sup>. Regardless of the age of these features, they occurred after the anthropogenic modification of the tooth. The uniform contrast between the interior of the marks and the adjacent areas supports the inference that anthropogenic modification happened before final burial and final mineralization of the tooth.

Teeth of megatheriids are composed of three tissues: vasodentine (inner layer), inner and outer orthodentine (middle layer), and cementum (outer layer)<sup>34,35</sup>; orthodentine is the hardest and thinnest bioapatite layer<sup>35</sup>. Dentinal tubules are parallel and aligned radially in the dentine matrix and can act as percolation paths for weathering or diagenetic fluids during fossilization<sup>34</sup>. Our synchrotron-based XRF imaging and X-ray computed ( $\mu$ CT) results confirm the nature of these dentine tubules, which were previously misidentified as anthropogenic marks<sup>18,19</sup>.

The chemical alteration observed through our SEM-EDS and XRF analysis (Figs. 6 and 7) indicates sedimentary filling and infiltration of exogenous elements in the dentine in the burial environment. The higher Sr/Ca ratio (Fig. 7E–F) suggests that the Sr incorporated in the tooth is likely diagenetic. The elements Fe, Mn, Al, Si, and Rb are uncommon components of dentine at the observed intensities, so their presence in the fossil tooth likely represents incorporation from the burial environment<sup>36,37</sup>. While we can observe Al, Si, and O from our SEM-EDS analyses (Fig. 6C–E), the elemental XRF distribution maps show that Fe and Rb have also infiltrated the dentinal tubules (Fig. 7). This pattern of infiltration is comparable to the results of Larmon et al.<sup>35</sup>, who investigated how diagenesis affected an *Eremotherium* tooth under cathodoluminescence analysis. These authors observed that the cementum and vasodentine layers of the tooth are highly susceptible to diagenesis, while orthodentine is the most resistant and therefore least altered layer. Regarding our Brazilian ground sloth tooth, the sediments possibly controlled Rb incorporation, which is commonly associated with clay minerals and micas<sup>38</sup>. Fe also likely came from the surrounding sediments, as it is commonly taken into fossil bones and teeth during diagenesis<sup>37</sup> or weathering<sup>39</sup>. Al, Si, and O suggest contamination from aluminosilicates from mineral clays, which are common in tank deposits in the northeast region of Brazil<sup>16,40,41</sup>. As the mineralogical composition of tank deposits results from the decomposition of the surrounding rocks<sup>16</sup>, the exogenous elements infiltrated in the dentine likely originated from clays as run-off water percolated through the rock. Additional sedimentological studies of this tank location are needed to clarify the origin of aluminosilicates in the environment.

Our study supports anthropogenic modification of ground sloth tooth (LPUS 4992), and that this modification occurred prior to final burial. However, it is also important to acknowledge the current limitations of our interpretations. Firstly, as tank deposits can be formed by different sedimentation events through time, their fossil assemblage can represent a mixture of different-age elements. Therefore, we cannot assert the exact timing of human modification of this material, which limits broader interpretations of human-megafauna interaction around 13,000 years ago in this locality.

The study of anthropogenic modification of teeth is still poorly explored, as most studies over the past four decades have focused on bone modifications. However, recent studies and experimental research have highlighted the importance of including teeth as potential human artifacts. Although somewhat unusual, human modification of teeth is known in the archaeological record, and animal teeth can be interpreted as transformed tools, retouchers<sup>42–46</sup>, and personal ornaments<sup>4,47</sup>. Anthropogenic marks on human teeth, from the Paleolithic to the Neolithic, have also been interpreted as resulting from funerary and cannibalistic practices<sup>48</sup>. This highlights that the anthropogenic modification of dental elements should be given greater consideration in the future.

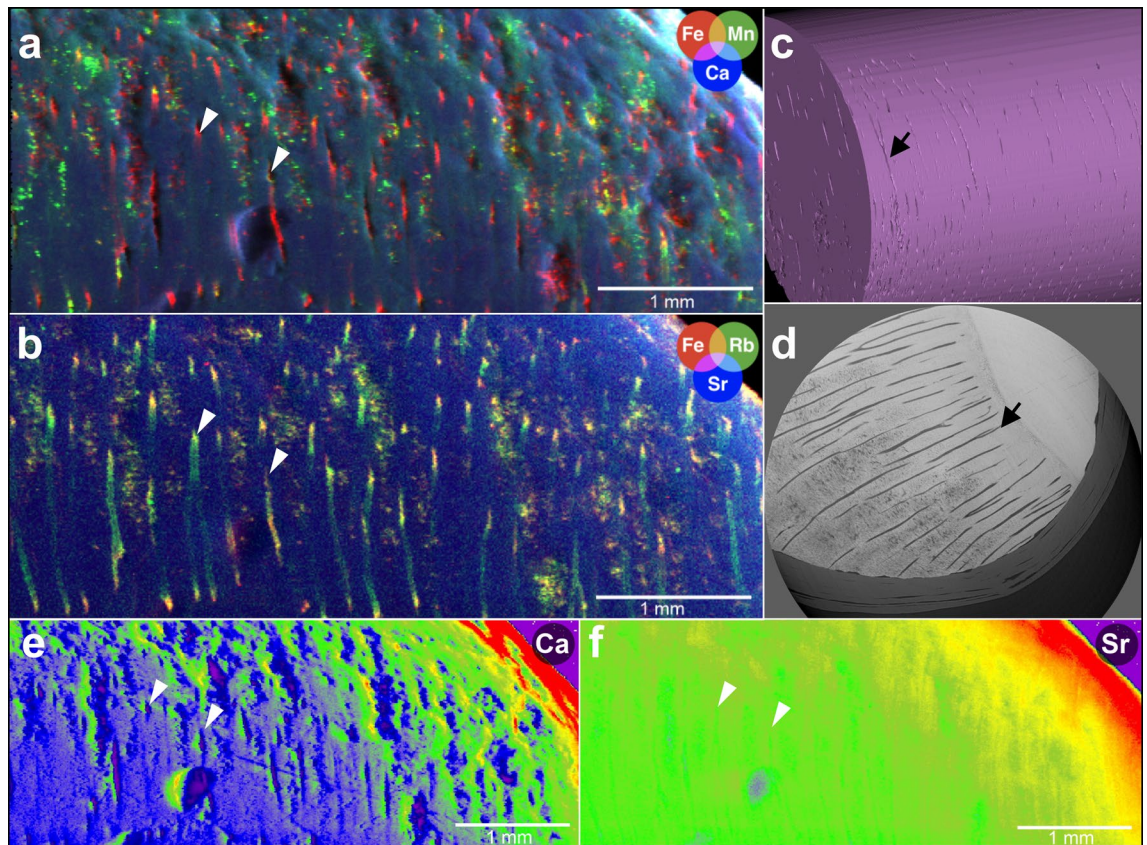


**Figure 7.** Exposed dentinal tubules analyzed under synchrotron XRF and microCT. (a, b) Synchrotron XRF highlights the incorporation of trace elements. False colors and captions: Ca in blue, Mn in green, and Fe in red (a), and Sr in blue, Fe in green, and Rb in red (b). (c, d) The nature of these structures is confirmed using microtomography and 3D image reconstructions (histological microstructures indicated by black arrows). Notice the distinct elemental distribution map between Ca (e) and Sr (f), and the incorporation pattern of Sr in the dentinal tubules. White arrows reference histological structures.

Our discussion about the human purpose for modifying this ground sloth tooth from Brazil is limited, especially due to the absence of specific traces related to the *chaîne opératoire* of the artifact production. We can only infer that the proposed artifact was reshaped for non-subsistence purposes. This evidence manifests the past human behavior and their relationship with the ecosystem, highlighting human perception of the surrounding fauna not only as prey or competitors in the landscape, but also as potential resources for technology and symbolic transformation.

Anthropogenic modification of teeth and mandibles of Pleistocene megamammals in the Americas is suggested through evidence from *Toxodon* in Brazil<sup>49</sup>, *Notiomastodon*, *Toxodon*, *Macrauchenia*, and *Lestodon* in Argentina<sup>50</sup>, and *Mastodon* in the USA<sup>51</sup>. Details of human-megafauna interaction in the Americas during the late Quaternary remain highly debated, especially for South America, where remarkable evidence for megafauna exploitation has been growing<sup>52</sup>. In this context, the currently available and any future evidence regarding tooth modification can contribute, together with bone surface modifications, to broader paleoecological and archaeological discussions in this continent.

We highlight in this study the scientific benefit of using different analytic methods and multidisciplinary approaches not only to distinguish human versus non-human taphonomic modification of bones and teeth, but also to determine the order of taphonomic processes and to support the interpretation of the timing of ancient modifications. The use of different techniques can provide distinct and complementary evidence (Fig. 2; Supplementary Table S1). Whereas SEM allows observation of internal microstructures and the external topography of the tooth surface and its taphonomic signatures,  $\mu$ CT allows the identification of histological features and 3D reconstruction of the tooth fragment and taphonomic signatures. On the other hand, UV/PL allows us to observe the marks' distribution, orientation, and their overlapping patterns, while EDS and XRF enable a detailed elemental characterization.

We note that the use of XRF is advantageous for differentiating diagenetically altered bioapatite layers and thus providing more reliable data for additional studies, such as stable isotopic analysis. Likewise, the use of PL is also beneficial, as it allows the detection of recent contamination in areas of interest for additional analysis (e.g. glue and other recent organic contamination; Fig. 4D). In addition, the development of novel approaches to studying zooarchaeological and paleontological materials supports growing cutting-edge research in this area. The more access researchers have to a range of novel techniques (e.g., synchrotron facilities worldwide), and/or collaboration with researchers in related expertise, the more feasible it will be to explore such taphonomic questions.

Although new approaches show great potential for exploring out-of-context materials that preserve disputed evidence, using such techniques presents challenges such as limited access and sometimes high cost of laboratories with high-resolution microscopes and synchrotron light equipment. Researchers will need to carefully assess the benefits of these methods and prioritize analyses of specific materials, such as (1) specimens with potentially important information found out of context, or whose stratigraphic information has been lost, especially from decades-old museum collections that are poorly documented; and (2) zooarchaeological or paleontological objects with major implications for current scientific paradigms, such as human origins and dispersal.

## Methods

The teeth of extinct, large-bodied sloths are bilophodont (two cusps), hypselodont (ever-growing and rootless), and lack enamel tissues<sup>53</sup>. The fragmentary molariform ground sloth tooth (LPUS 4992) analyzed in this study (Fig. 1C) presents these characteristics and is housed at the Laboratório de Paleontologia of the Universidade Federal de Sergipe (UFS), Brazil. It has not undergone any chemical preparation; it has only been brushed, washed with water, and later glued after breakage. The only previous analyses were digital microscopic images and radiocarbon dating on bioapatite<sup>18,19</sup>. Here, we identified surface modifications based on criteria in the published literature and the study of comparative specimens housed at the Smithsonian's National Taphonomic Reference Collection (NTRC) (Table 1; Fig. S3; supplementary material). We performed imaging and elemental analyses on this material through six techniques: stereomicroscopy, SEM, energy dispersive spectroscopy (EDS), photoluminescence spectral imaging (PL), XRF, and micro-computed tomography ( $\mu$ CT).

Stereomicroscopic images were taken using a stereomicroscope Nikon SMZ-25 at LNBio, Brazil. SEM images using a back-scattered electron mode (BSE-SEM) detector and EDS data (Fig. 5I; Fig. S1, supplementary material) were collected using the TM3000 tabletop microscope Hitachi, under low vacuum with an acceleration voltage of 15 kV, at the Laboratório de Pesquisa em Bioenergia e Materiais Lignocelulósicos, UFSCar, Brazil, without coating the specimen. SEM and EDS images (Fig. 6) were taken under low vacuum (~50 to 70 Pa), with an acceleration voltage of 15 kV, with Variable Pressure Secondary Electron (VPSE), using the Zeiss Supra 55VP FEG-SEM at IPANEMA, France.

The PL multispectral images were collected using the in-house developed setup at the IPANEMA laboratory in France. We collected reflectance images at the wavelength of  $472 \pm 30$  nm under 470 nm illumination (Fig. 4B); at the red (685 nm) domain under 470 nm illumination (Fig. 4C); and luminescence emissions in the blue (472 nm), green (514 nm), and red (685 nm) spectral domains under UV (385 nm) illumination (Fig. 4D). Figure 4A was collected in diffuse reflectance mode in the 535–607 nm range using the ambient light in the lab space. Scalar images were aligned using the template matching plugin in FIJI and combined into false-color RGB images using ImageJ for easier intercomparison (Fig. 4D).

Macroscopic Photoluminescence (PL) imaging is a novel imaging approach applied in the research of ancient materials which has been little explored in the study of bone or tooth surface modifications. Photoluminescence is the emission of light (in multiple wavelengths) after the absorption of photons of higher energy such as ultraviolet (UV) and can be used to observe contrasts in color representing variations in surface chemistry that are invisible to the naked eye<sup>54</sup>. The customized system we used allows optimal excitation and emission ranges to distinguish specific organic and inorganic structures. In practice, we used a tunable LED source and a multispectral detection to enhance contrasts between marks/features on target materials and differentiate their potential origins using PL properties<sup>55</sup>. The PL excitation and emission properties at the same peaks may depend on the reflected material components with different biological compositions (e.g., bioapatite, organic matter). In this study, we performed UV/PL analyses to detect surface chemistry variations on the fossil tooth that may distinguish ancient human modifications and/or subsequent non-anthropogenic taphonomic signatures. The integration of PL analysis has demonstrated a significant contribution to reconstructing the taphonomic history of this tooth. Luminescence emissions under UV illumination of the tooth generated distinct contrast imagery of taphonomic characteristics (Fig. 4A–D). Optimization of the excitation and emission wavelengths made it much easier to locate and identify the orientation of anthropogenic marks.

Synchrotron XRF raster-scanned images were collected at the PUMA beamline of the SOLEIL synchrotron in France. We mapped an area of the lateral edges of the tooth.  $10 \text{ mm} \times 4 \text{ mm}$  ( $H \times V$ ) maps were acquired in continuous scanning mode (“flyscan”) with  $10 \mu\text{m}$  resolution and 100 ms acquisition time. The incident beam was set to an energy of 18 keV. Spectral images were processed using the PyMca software<sup>56</sup> and a package in R developed by L. Bertrand and Serge Cohen (IPANEMA). The elemental distribution of biomineralized tissues mapped with synchrotron-based XRF imaging provides a better understanding of their original composition and diagenetic history<sup>57–59</sup>. Besides being non-invasive, which is highly important for zooarchaeological materials such as bones and teeth with anthropogenic modifications, one of the advantages of this technique is the high-resolution imaging maps that show the presence and distribution of low to high atomic mass elements in the fossil surface.

Synchrotron  $\mu$ CT was performed at the PSICHÉ beamline of the SOLEIL synchrotron in France<sup>60</sup>. Imaging was performed using pink beam illumination with average photon energy ~80 keV in two configurations: low resolution,  $5.85 \mu\text{m}$  pixel size and 180 mm propagation distance from the sample to the detector for phase contrast; and high resolution,  $1.3 \mu\text{m}$  pixel size with 80 mm propagation distance. Reconstructions were performed using PyHST2 software<sup>61</sup>, with Paganin filtering to improve signal-to-noise in phase contrast images<sup>62</sup>.  $\mu$ CT analysis is fundamental for exploring the internal microstructures of fossil materials in a non-destructive way. Synchrotron-based  $\mu$ CT provides an advantage over traditional microtomography due to the high contrast between materials obtained by exploiting propagation phase contrast, and the high intensity of the parallel beam<sup>63</sup>.  $\mu$ CT contrasts can be used semi-quantitatively toward material identification<sup>64</sup>. Besides detailed histological information, it

allows the three-dimensional observation and reconstruction of mark morphologies, which can complement stereomicroscopic and SEM characterizations of materials of taphonomic interest<sup>65,66</sup>.

## Data availability

All study data are available in included the article or the supplementary material.

Received: 12 March 2024; Accepted: 1 August 2024

Published online: 03 September 2024

## References

- Shipman, P. & Rose, J. Evidence of butchery and hominid activities at Torralba and Ambrona; an evaluation using microscopic techniques. *J. Archaeol. Sci.* **10**, 465–474 (1983).
- Shipman, P., Fisher, D. C. & Rose, J. Mastodon butchery: Microscopic evidence of carcass processing and bone tool use. *Paleobiology* **10**, 358–365 (1984).
- Olsen, S. L. & Shipman, P. Surface modification on bone: Trampling versus butchery. *J. Archaeol. Sci.* **15**, 535–553 (1988).
- Martisius, N. L. *et al.* Initial Upper Paleolithic bone technology and personal ornaments at Bacho Kiro Cave (Bulgaria). *J. Hum. Evol.* **167**, 103198 (2022).
- Fernandez-Jalvo, Y. & Andrews, P. *Atlas of Taphonomic Identifications: 1001+ Images of Fossil and Recent Mammal Bone Modification* (Springer, 2016). <https://doi.org/10.1007/978-94-017-7432-1>.
- Behrensmeyer, A. K., Gordon, K. D. & Yanagi, G. T. Trampling as a cause of bone surface damage and pseudo-cutmarks. *Nature* **319**, 768–771 (1986).
- Blumenschine, R. J., Marean, C. W. & Capaldo, S. D. Blind tests of inter-analyst correspondence and accuracy in the identification of cut marks, percussion marks, and carnivore tooth marks on bone surfaces. *J. Archaeol. Sci.* **23**, 493–507 (1996).
- Pesquero, M. D., Bell, L. S. & Fernández-Jalvo, Y. Skeletal modification by microorganisms and their environments. *Hist. Biol.* **30**, 882–893 (2018).
- Braun, D. R., Pante, M. & Archer, W. Cut marks on bone surfaces: Influences on variation in the form of traces of ancient behaviour. *Interface Focus* **6**, 20160006 (2016).
- Shipman, P. Applications of Scanning Electron Microscopy to Taphonomic Problems\*. *Ann. N. Y. Acad. Sci.* **376**, 357–385 (1981).
- Parfitt, S. A. & Bello, S. M. Bone tools, carnivore chewing and heavy percussion: Assessing conflicting interpretations of Lower and Upper Palaeolithic bone assemblages. *R. Soc. Open Sci.* **11**, 231163 (2024).
- Domínguez-Rodrigo, M., De Juana, S., Galán, A. B. & Rodríguez, M. A new protocol to differentiate trampling marks from butchery cut marks. *J. Archaeol. Sci.* **36**, 2643–2654 (2009).
- James, E. C. & Thompson, J. C. On bad terms: Problems and solutions within zooarchaeological bone surface modification studies. *Environ. Archaeol.* **20**, 89–103 (2015).
- Pante, M. C. *et al.* A new high-resolution 3-D quantitative method for identifying bone surface modifications with implications for the Early Stone Age archaeological record. *J. Hum. Evol.* **102**, 1–11 (2017).
- Otárola-Castillo, E. *et al.* Differentiating between cutting actions on bone using 3D geometric morphometrics and Bayesian analyses with implications to human evolution. *J. Archaeol. Sci.* **89**, 56–67 (2018).
- Araújo-Júnior, H. I. D., Porpino, K. D. O., Ximenes, C. L. & Bergqvist, L. P. Unveiling the taphonomy of elusive natural tank deposits: A study case in the Pleistocene of northeastern Brazil. *Palaeogeogr. Palaeoclimatol. Palaeoecol.* **378**, 52–74 (2013).
- França, L. D. M., Araújo-Júnior, H. I. D. & Dantas, M. A. T. Taphonomy, paleoecology and chronology of a late Quaternary tank (natural reservoir) deposit from the Brazilian Intertropical Region. *Quat. Sci. Rev.* **313**, 108199 (2023).
- Dantas, M. A. T., De Queiroz, A. N., Vieira Dos Santos, F. & Cozzuol, M. A. An anthropogenic modification in an Eremotherium tooth from northeastern Brazil. *Quat. Int.* **253**, 107–109 (2012).
- Dantas, M. A. T. *et al.* Dated evidence of the interaction between humans and megafauna in the late Pleistocene of Sergipe state, northeastern Brazil. *Quat. Int.* **352**, 197–199 (2014).
- Dantas, M. A. T. & Cherkinsky, A. Interrelation of radiocarbon ages from bone fractions in the Brazilian Intertropical Region. *Quat. Res.* **115**, 202–206 (2023).
- França, L. M., Dantas, M. A. T., Zucon, M. H. & Cozzuol, M. A. *Megafauna do Pleistoceno final da fazenda São José, Poço Redondo, Sergipe, Brasil* 21 (Springer, 2011).
- França, L. M. *et al.* Chronology and ancient feeding ecology of two upper Pleistocene megamammals from the Brazilian Intertropical Region. *Quat. Sci. Rev.* **99**, 78–83 (2014).
- Dantas, M. A. T. *et al.* Isotopic paleoecology of the Pleistocene megamammals from the Brazilian Intertropical Region: Feeding ecology ( $\delta^{13}\text{C}$ ), niche breadth and overlap. *Quat. Sci. Rev.* **170**, 152–163 (2017).
- Hubbe, A., Haddad-Martim, P. M., Hubbe, M. & Neves, W. A. Comments on: An anthropogenic modification in an Eremotherium tooth from northeastern Brazil. *Quat. Int.* **269**, 94–96 (2012).
- Cartelle, C. & De Iuliis, G. *Eremotherium laurillardii*: The panamerican late Pleistocene megatheriid sloth. *J. Vertebr. Paleontol.* **15**, 830–841 (1995).
- Cartelle, C., De-Iuliis, G. & Pujos, F. *Eremotherium laurillardii* (Lund, 1842) (Xenarthra, Megatheriinae) is the only valid megatheriine sloth species in the Pleistocene of intertropical Brazil: A response to Faure *et al.*, 2014. *Compt. Rend. Palevol.* **14**, 15–23 (2015).
- Marin-Monfort, M. D., Suñer, M. & Fernández-Jalvo, Y. Characterization of recent marks produced on fossil bone surface during sullegic and trephic processes and their influence on taphonomic studies. *Quat. Int.* **481**, 3–13 (2018).
- Irmis, R. B. & Elliott, D. K. Taphonomy of a Middle Pennsylvanian marine vertebrate assemblage and an actualistic model for marine abrasion of teeth. *PALAIOS* **21**, 466–479 (2006).
- Shipman, P. & Rose, J. Early hominid hunting, butchering, and carcass-processing behaviors: Approaches to the fossil record. *J. Anthropol. Archaeol.* **2**, 57–98 (1983).
- Marginedas, F., Rodríguez-Hidalgo, A. & Saladié, P. Rodent gnawing over fresh, dry and thermo altered bones: An experimental study with archaeological implications at El Mirador Cave (Atapuerca, Spain). *Hist. Biol.* **35**, 1470–1483 (2023).
- Knüsel, C. J. & Robb, J. Funerary taphonomy: An overview of goals and methods. *J. Archaeol. Sci. Rep.* **10**, 655–673 (2016).
- Micó, C. *et al.* Differentiating taphonomic features from trampling and dietary microwear, an experimental approach. *Hist. Biol.* **2023**, 1–23 (2023).
- Wrobel, G. D. & Biggs, J. Osteophageous insect damage on human bone from Je'reftheel, a Maya mortuary cave site in west-central Belize. *Int. J. Osteoarchaeol.* **28**, 745–756 (2018).
- Kalthoff, D. C. Microstructure of dental hard tissues in fossil and recent xenarthrans (Mammalia: Folivora and Cingulata). *J. Morphol.* **272**, 641–661 (2011).
- Larmon, J. T., McDonald, H. G., Ambrose, S., DeSantis, L. R. G. & Lucero, L. J. A year in the life of a giant ground sloth during the Last Glacial Maximum in Belize. *Sci. Adv.* **5**, eaau1200 (2019).

36. Carvalho, M. L., Marques, A. F., Marques, J. P. & Casaca, C. Evaluation of the diffusion of Mn, Fe, Ba and Pb in Middle Ages human teeth by synchrotron microprobe X-ray fluorescence. *Spectrochim. Acta Part B At. Spectrosc.* **62**, 702–706 (2007).
37. Zougrou, I. M. *et al.* Influence of depositional environment in fossil teeth: A micro-XRF and XAFS study. *J. Phys. Conf. Ser.* **499**, 012015 (2014).
38. Dypvik, H. & Harris, N. B. Geochemical facies analysis of fine-grained siliciclastics using Th/U, Zr/Rb and (Zr+Rb)/Sr ratios. *Chem. Geol.* **181**, 131–146 (2001).
39. Bao, H., Koch, P. L. & Hepple, R. P. Hematite and calcite coatings on fossil vertebrates. *J. Sediment. Res.* **68**, 727–738 (1998).
40. Carvalho-Laurentino, J. C. S., Porpino, K. O. & Araújo-Júnior, H. I. Integrating fossil diagenesis and geochemistry in the paleoenvironmental reconstruction of a tank deposit bearing quaternary vertebrates in Northeastern Brazil. *Ameghiniana* **59**, 274–296 (2022).
41. Prado-de-Oliveira-Martins, G., de-Araújo-Júnior, H. I., dos-Santos, A. C. & Porpino, K. O. Quaternary megafauna bone diagenesis preserved in natural tank deposits from Brazil: Taphonomic and paleoenvironmental aspects. *J. South Am. Earth Sci.* **119**, 103984 (2022).
42. Castel, J.-C., Chauvière, F.-X. & Madelaine, S. Sur os et sur dents: Les “retouchoirs” aurignaciens de la Ferrassie (Savignac-de-Miremont, Dordogne). *PALEO Rev. Archéol. Préhistorique* **2003**, 29–50 (2003).
43. Abrams, G. Palaeolithic bone retouchers from Belgium: A preliminary overview of the recent research through historic and recently excavated bone collections. *Orig. Bone Tool Technol.* **2018**, 197–213 (2018).
44. Gilson, S.-P., Gates-St-Pierre, C., Lominy, M. & Lessa, A. Shark teeth used as tools: An experimental archaeology study. *J. Archaeol. Sci. Rep.* **35**, 102733 (2021).
45. Bello, S. M., Crété, L., Galway-Witham, J. & Parfitt, S. A. Knapping tools in Magdalenian contexts: New evidence from Gough's Cave (Somerset, UK). *PLOS ONE* **16**, e0261031 (2021).
46. Micó, C. *et al.* Using horse teeth to shape stone tools: An experimental approach to characterise use-wear traces. *Archaeol. Anthropol. Sci.* <https://doi.org/10.1007/s12520-024-01988-5> (2024).
47. Tejero, J.-M. *et al.* New insights into the Upper Palaeolithic of the Caucasus through the study of personal ornaments. Teeth and bones pendants from Satsurbliá and Dzudzuana caves (Imereti, Georgia). *PLOS ONE* **16**, e0258974 (2021).
48. Crété, L., Parfitt, S. A., Day, C. & Bello, S. M. Non-masticatory striations on human teeth from the British Upper Palaeolithic to the Neolithic. *Human. Soc. Sci. Commun.* **11**, 61 (2024).
49. Barros-Barreto, C. *et al.* Abismo Ponta de Flecha: Um projeto arqueológico, paleontológico e geológico no médio Ribeira de Iguape SP. *Sao Paulo Rev. Pré-História* **3**, 195–215 (1982).
50. Toledo, M. J. Anthropogenic modifications on megafauna bones in the paleontological collections of the Museum national d'Histoire naturelle de Paris: Historical aspects and implications for the Pampean Pleistocene peopling. *L'Anthropologie* **127**, 103134 (2023).
51. Brush, N. *et al.* Description of an American Mastodon (*Mammot americanum*) Site in Morrow County, Ohio, and assessment of evidence for Early Paleoindian exploitation. *Archaeol. East. N. Am.* **46**, 215–240 (2018).
52. Bampi, H., Barberi, M. & Lima-Ribeiro, M. S. Megafauna kill sites in South America: A critical review. *Quat. Sci. Rev.* **298**, 107851 (2022).
53. Green, J. L. & Kalthoff, D. C. Xenarthran dental microstructure and dental microwear analyses, with new data for *Megatherium americanum* (Megatheriidae). *J. Mammal.* **96**, 645–657 (2015).
54. Frese, M., Gloy, G., Oberprieler, R. G. & Gore, D. B. Imaging of Jurassic fossils from the Talbragar Fish Bed using fluorescence, photoluminescence, and elemental and mineralogical mapping. *PLOS ONE* **12**, e0179029 (2017).
55. Thoury, M. *et al.* High spatial dynamics-photoluminescence imaging reveals the metallurgy of the earliest lost-wax cast object. *Nat. Commun.* **7**, 13356 (2016).
56. Solé, V. A., Papillon, E., Cotte, M., Walter, Ph. & Susini, J. A multiplatform code for the analysis of energy-dispersive X-ray fluorescence spectra. *Spectrochim. Acta Part B At. Spectrosc.* **62**, 63–68 (2007).
57. Dumont, M. *et al.* Synchrotron XRF analyses of element distribution in fossilized sauropod dinosaur bones. *Powder Diffr.* **24**, 130–134 (2009).
58. Gueriau, P. & Bertrand, L. Deciphering exceptional preservation of fossils through trace elemental imaging. *Microsc. Today* **23**, 20–25 (2015).
59. Dean, C., Le Cabec, A., Spiers, K., Zhang, Y. & Garrevoet, J. Incremental distribution of strontium and zinc in great ape and fossil hominin cementum using synchrotron X-ray fluorescence mapping. *J. R. Soc. Interface* **15**, 20170626 (2018).
60. King, A. *et al.* Tomography and imaging at the PSICHE beam line of the SOLEIL synchrotron. *Rev. Sci. Instrum.* **87**, 093704 (2016).
61. Mirone, A., Brun, E., Gouillart, E., Tafforeau, P. & Kieffer, J. The PyHST2 hybrid distributed code for high speed tomographic reconstruction with iterative reconstruction and a priori knowledge capabilities. *Nucl. Instrum. Methods Phys. Res. Sect. Accel. Spectrometers Detect. Assoc. Equip.* **324**, 41–48 (2014).
62. Paganin, D., Mayo, S. C., Gureyev, T. E., Miller, P. R. & Wilkins, S. W. Simultaneous phase and amplitude extraction from a single defocused image of a homogeneous object. *J. Microsc.* **206**, 33–40 (2002).
63. Stampanoni, M. *et al.* High resolution X-ray detector for synchrotron-based microtomography. *Nucl. Instrum. Methods Phys. Res. Sect. Accel. Spectrometers Detect. Assoc. Equip.* **491**, 291–301 (2002).
64. Maldanis, L. *et al.* Nanoscale 3D quantitative imaging of 1.88 Ga Gunflint microfossils reveals novel insights into taphonomic and biogenic characters. *Sci. Rep.* **10**, 8163 (2020).
65. Bello, S. M. & Galway-Witham, J. Bone taphonomy inside and out: Application of 3-dimensional microscopy, scanning electron microscopy and micro-computed tomography to the study of humanly modified faunal assemblages. *Quat. Int.* **517**, 16–32 (2019).
66. Pansani, T. R. *et al.* Evidence of artefacts made of giant sloth bones in central Brazil around the last glacial maximum. *Proc. R. Soc. B Biol. Sci.* **290**, 20230316 (2023).

## Acknowledgements

We acknowledge SOLEIL for the provision of synchrotron radiation facilities under project number 20210012, and DNPM/ANM for permission for the temporary exportation of the fossil material from Brazil to France (process number 48051.000270/2021-84). The authors are thankful to Irma Yamamoto (ANM), Fabiana Silva Vieira (UFS), and Alexander Liparini (UFMG) for the support in accessing the material; Maëva l'Heronde (IPANEMA) for assistance during SEM analysis; Pierre Gueriau (IPANEMA) for assistance with  $\mu$ CT and XRF data collection, rendering and interpretation; Douglas Galante and Murilo de Carvalho for the access to the in-house microscopic equipment at the Brazilian Biosciences National Laboratory (LNBio)/Brazilian Centre for Research in Energy and Materials (CNPEM); and Felipe Waldherr for help with the map figure. TRP appreciates Yolanda Fernandez-Jalvo and Cristian Cipó for the fruitful discussions and encouragement of this work. Thank you to the two anonymous reviewers whose constructive suggestions helped us to improve the quality of this work.

### Author contributions

TRP designed the study during part of her doctorate degree. TRP acquired optical microscopy, scanning electron microscopy, and energy-dispersive spectroscopy data and prepared images. TRP and MT performed photoluminescence analyses and prepared images. TRP, LB, and SS performed synchrotron X-ray fluorescence analysis and prepared images. TRP and AK performed synchrotron microtomography analysis and prepared images. TRP visited the NTRC (Smithsonian Institution) for taphonomic comparison, under the supervision of AKB and BP. TRP, MLAFP, BP, AKB, MATD, LB, LA, and HIAJ contributed to taphonomic interpretation. TRP wrote the original draft and all authors reviewed the manuscript text, images, and tables.

### Funding

This work were funded by Coordenação de Aperfeiçoamento de Pessoal de Nível Superior (Grant no. 88887.569989/2020-00), UFSCar PrInt, Peter Buck Postdoctoral Fellowship–Smithsonian Institution, Conselho Nacional de Desenvolvimento Científico e Tecnológico (Grant no. 420424/2023-7), and Fundação de Amparo à Pesquisa do Estado de São Paulo (Grant no. 2023/04501-6).

### Competing interests

The authors declare no competing interests.

### Additional information

**Supplementary Information** The online version contains supplementary material available at <https://doi.org/10.1038/s41598-024-69145-5>.

**Correspondence** and requests for materials should be addressed to T.R.P.

**Reprints and permissions information** is available at [www.nature.com/reprints](http://www.nature.com/reprints).

**Publisher's note** Springer Nature remains neutral with regard to jurisdictional claims in published maps and institutional affiliations.

**Open Access** This article is licensed under a Creative Commons Attribution-NonCommercial-NoDerivatives 4.0 International License, which permits any non-commercial use, sharing, distribution and reproduction in any medium or format, as long as you give appropriate credit to the original author(s) and the source, provide a link to the Creative Commons licence, and indicate if you modified the licensed material. You do not have permission under this licence to share adapted material derived from this article or parts of it. The images or other third party material in this article are included in the article's Creative Commons licence, unless indicated otherwise in a credit line to the material. If material is not included in the article's Creative Commons licence and your intended use is not permitted by statutory regulation or exceeds the permitted use, you will need to obtain permission directly from the copyright holder. To view a copy of this licence, visit <http://creativecommons.org/licenses/by-nc-nd/4.0/>.

© The Author(s) 2024